



Biogenic cloud nuclei in the central Amazon during the transition from wet to dry season

James D. Whitehead¹, Eoghan Darbyshire¹, Joel Brito², Henrique M. J. Barbosa², Ian Crawford¹, Rafael Stern³, Martin W. Gallagher¹, Paul H. Kaye⁴, James D. Allan¹, Hugh Coe¹, Paulo Artaxo², and Gordon McFiggans¹

¹Centre for Atmospheric Science, SEES, University of Manchester, Oxford Road, Manchester, UK

²Institute of Physics, University of São Paulo, Rua do Matão, Travessa R, 187, CEP 05508-090, São Paulo, Brazil

³Instituto Nacional de Pesquisas da Amazônia, Av. André Araújo, 2936, Aleixo, CEP 69060-001, Manaus, Brazil

⁴Science and Technology Research Institute, University of Hertfordshire, Hertfordshire, UK

Correspondence to: Gordon McFiggans (g.mcfiggans@manchester.ac.uk)

Received: 15 December 2015 – Published in Atmos. Chem. Phys. Discuss.: 18 January 2016

Revised: 7 June 2016 – Accepted: 14 July 2016 – Published: 3 August 2016

Abstract. The Amazon basin is a vast continental area in which atmospheric composition is relatively unaffected by anthropogenic aerosol particles. Understanding the properties of the natural biogenic aerosol particles over the Amazon rainforest is key to understanding their influence on regional and global climate. While there have been a number of studies during the wet season, and of biomass burning particles in the dry season, there has been relatively little work on the transition period – the start of the dry season in the absence of biomass burning. As part of the Brazil–UK Network for Investigation of Amazonian Atmospheric Composition and Impacts on Climate (BUNIAACIC) project, aerosol measurements, focussing on unpolluted biogenic air masses, were conducted at a remote rainforest site in the central Amazon during the transition from wet to dry season in July 2013. This period marks the start of the dry season but before significant biomass burning occurs in the region.

Median particle number concentrations were 266 cm^{-3} , with size distributions dominated by an accumulation mode of 130–150 nm. During periods of low particle counts, a smaller Aitken mode could also be seen around 80 nm. While the concentrations were similar in magnitude to those seen during the wet season, the size distributions suggest an enhancement in the accumulation mode compared to the wet season, but not yet to the extent seen later in the dry season, when significant biomass burning takes place. Submicron nonrefractory aerosol composition, as measured by an aerosol chemical speciation monitor (ACSM), was dominated by organic material (around 81 %). Aerosol hygro-

scopicity was probed using measurements from a hygroscopicity tandem differential mobility analyser (HTDMA), and a quasi-monodisperse cloud condensation nuclei counter (CCNc). The hygroscopicity parameter, κ , was found to be low, ranging from 0.12 for Aitken-mode particles to 0.18 for accumulation-mode particles. This was consistent with previous studies in the region, but lower than similar measurements conducted in Borneo, where κ ranged 0.17–0.37.

A wide issue bioaerosol sensor (WIBS-3M) was deployed at ground level to probe the coarse mode, detecting primary biological aerosol by fluorescence (fluorescent biological aerosol particles, or FBAPs). The mean FBAP number concentration was $400 \pm 242\text{ L}^{-1}$; however, this ranged from around 200 L^{-1} during the day to as much as 1200 L^{-1} at night. FBAPs dominated the coarse-mode particles, comprising between 55 and 75 % of particles during the day to more than 90 % at night. Non-FBAPs did not show a strong diurnal pattern. Comparison with previous FBAP measurements above canopy at the same location suggests there is a strong vertical gradient in FBAP concentrations through the canopy. Cluster analysis of the data suggests that FBAPs were dominated (around 70 %) by fungal spores. Further, long-term measurements will be required in order to fully examine the seasonal variability and distribution of primary biological aerosol particles through the canopy.

This is the first time that such a suite of measurements has been deployed at this site to investigate the chemical composition and properties of the biogenic contributions to Amazonian aerosol during the transition period from the wet to

the dry season, and thus provides a unique comparison to the aerosol properties observed during the wet season in previous similar campaigns. This was also the first deployment of a WIBS in the Amazon rainforest to study coarse-mode particles, particularly primary biological aerosol particles, which are likely to play an important role as ice nuclei in the region.

1 Introduction

The Amazon basin consists of the world's largest rainforest, covering an area of 5.5 million km². The Amazon rainforest is one of the few continental regions where atmospheric processes are minimally influenced by anthropogenic emissions, particularly during the wet season, and ambient conditions can represent, to some extent, those of the pristine pre-industrial era (Pöschl et al., 2010). Concentrations and properties of aerosol particles are largely governed by biogenic emissions of both primary biological aerosol particles (PBAP) and biogenic volatile organic compounds (BVOCs), which contribute to secondary organic aerosol (SOA). On a regional scale, in the wet season, the hydrological cycle is strongly influenced by these biogenic aerosol emissions, which provide most of the cloud condensation nuclei and thereby influence the radiation balance and cloud lifetime (Pöschl et al., 2010). In the dry season, by contrast, widespread biomass burning can result in a substantially increased aerosol optical depth over large areas of Amazonia, as well as modified cloud properties and suppressed precipitation (Andreae et al., 2004).

Previous studies in the pristine Amazon rainforest showed that fine particles (which account for most of the cloud condensation nuclei) consist mostly of secondary organic material derived from oxidized biogenic gases (Pöschl et al., 2010; Martin et al., 2010a; Allan et al., 2014; Chen et al., 2015). A lack of evidence for new particle formation during ground-based measurements (Zhou et al., 2002; Rissler et al., 2004; Martin et al., 2010a) implies that nucleation processes occur at higher altitudes, and new particles are entrained into the boundary layer from aloft (Krejci et al., 2005; Martin et al., 2010b). Larger supermicron particles are dominated by primary biological aerosol particles (PBAP) released from rainforest biota (Elbert et al., 2007; Pöschl et al., 2010; Huffman et al., 2012), which can play a significant role as ice nuclei (Prenni et al., 2009). These PBAP consist of wind-driven particles, such as pollen, bacteria, and plant debris, as well as actively ejected material, such as fungal and plant spores. Nonbiological particles observed in the Amazon in the supermicron size range largely consist of advected Saharan dust and sea salt from the Atlantic (Formenti et al., 2001; Worobiec et al., 2007; Martin et al., 2010b).

The low aerosol number concentrations in the pristine Amazon rainforest (typically a few hundred cm⁻³) mean that CCN activation in convective clouds is often aerosol limited

(Pöschl et al., 2010). It is clear that there is a strong coupling between the rainforest biosphere and the hydrological cycle in the Amazon basin, with biogenic aerosol particles providing the nuclei for clouds, which, in turn, sustain the rainforest through precipitation (Pöschl et al., 2010).

Improving our knowledge of these processes is necessary for understanding the influence the Amazon rainforest has on regional and global climate and atmospheric composition, and how changing land use and climate in Amazonia will impact this (Artaxo et al., 2013). To this end, the Brazil–UK Network for Investigation of Amazonian Atmospheric Composition and Impacts on Climate (BUNIAACIC) was established to define and nurture a framework within which future UK contributions to studies in these areas may be coordinated. As part of the BUNIAACIC project, a short-term intensive measurement campaign was undertaken at a pristine rainforest site in July 2013. The main focus of this study was to look at natural (biogenic) aerosol at this site at the beginning of the dry season (also referred to as the transition from wet to dry season), and to compare to previous measurements made during the wet season at the same location (Martin et al., 2010a). Here, we present the results of this study.

2 Methodology

2.1 Measurement site and sampling

The measurements were conducted at a remote site in the pristine Amazonian rainforest between 4 and 28 July 2013, during the transition from the wet to dry season. This is around the start of the dry season but before significant biomass burning takes place. In July 2013, the total rainfall measured was 153 mm, mostly concentrated at the start and end of the month (during the measurement period itself, the rainfall was 77 mm). For the purposes of comparison, the AMAZE-08 campaign, which was conducted at the same site, had 370 mm of rainfall over the course of 5 weeks during the wet season (Martin et al., 2010a). In this study, the quartile ranges in temperature were 24–29 °C during the daytime, and 23–25 °C at night; relative humidity (RH) was 72–92 % by day and 85–96 % at night. By contrast, the conditions during AMAZE-08 were cooler and more humid, with temperature ranging 23–27 °C during the day and 22–24 °C at night; RH ranging 88–99 % by day and 96–100 % at night (Martin et al., 2010a).

Sampling was done at the TT34 tower (2°35'40" S, 60°12'33" W; elevation 110 m), in the Reserva Biológica do Cuieiras, approximately 60 km NNW of the city of Manaus in Brazil (see Fig. 1). The site is representative of near-pristine conditions, and no biomass burning takes place within the reservation; however, the site can be affected by regional transport of pollutants including emissions from Manaus and biomass burning (Artaxo et al., 2013; Rizzo

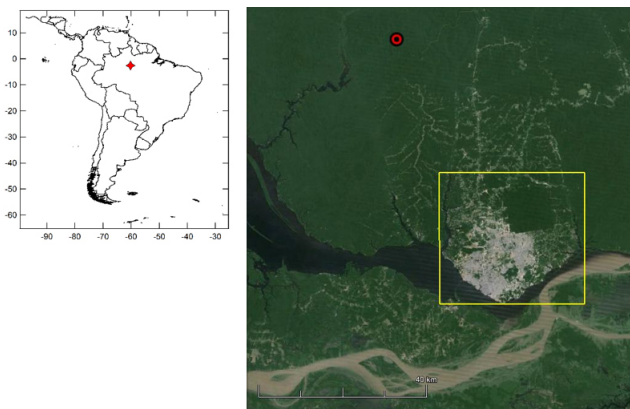


Figure 1. Location of the sampling site, shown by the red markers. The yellow rectangle represents the bounding box around Manaus used to flag air masses influenced by pollution from the city.

et al., 2013). Locally, accommodation for researchers and a 60 kW diesel generator were situated 0.33 and 0.72 km, respectively, in a WNW direction from the tower. Intensive measurement campaigns have taken place at this site in the past (e.g. Martin et al., 2010a), and long-term measurements have been conducted since 2008 (Artaxo et al., 2013; Rizzo et al., 2013). During this experiment, local time was 4 h behind UTC.

A laminar sample flow of about 17 L min^{-1} was drawn through a 3/4 in. OD stainless steel line from a height of 39 m (about 10 m above canopy height) down to a ground-level air-conditioned container, in which the instruments were housed. Before entering the container, the sample was passed through an automatic regenerating adsorption aerosol dryer (Tuch et al., 2009). This kept the RH in the sample flow between 20 and 40 %. For the range of flows rates during this campaign the transmission range has previously been calculated from 4 nm to $7\text{ }\mu\text{m}$ (Martin et al., 2010a). Instruments drawing off this dried sample flow included a hygroscopicity tandem differential mobility analyser (HTDMA; University of Manchester), and a cloud condensation nuclei counter (CCNc; CCN-100, Droplet Measurement Technologies). Upstream from these instruments, the sample flow (2 L min^{-1}) was further dried to an RH of between 15 and 25 % with a Nafion dryer operating with a counterflow of dry compressed air. The flow then passed through an electrical ionizer (model 1090, MSP Corporation), providing a charge-neutralized aerosol sample to the instruments. These same instruments were deployed in Borneo during the OP3 project (Irwin et al., 2011). Further details of the HTDMA and CCNc are given below.

Core instruments running at the site, on the same inlet, included a multi-angle absorption photometer (MAAP; model 5012, Thermo-Scientific), a condensation particle counter (CPC; model 3772, TSI), and an aerosol chemical speciation monitor (ACSM; Aerodyne Research Inc.). The ACSM

was used to measure mass concentrations of particulate ammonium, nitrate, sulfate, chloride, and organic species in the submicron size range. Mass calibration was obtained by sampling monodisperse ammonium nitrate and ammonium sulfate. The instrument collection efficiency was calculated to be 1 during BUNIAACIC, through the comparison of the mass concentration of species measured by the ACSM and MAAP (black carbon equivalent; BC_e) with the integrated mass of the SMPS. Further instrumental details and data post-processing is given by Brito et al. (2014). A weather station (Davis, USA) at the top of the tower provided meteorological data (wind speed and direction, temperature, RH, etc.).

As well as the instruments in the container, a wide issue bioaerosol sensor (WIBS; model 3M, University of Hertfordshire) was operated in a weatherproof box on the ground, a short distance from the base of the tower, with a short (1 m) 1/4 in. OD stainless steel inlet (more details are provided below). Other core instruments running at the site, but not used in this study, are detailed by Artaxo et al. (2013).

2.2 HTDMA measurements

In the HTDMA (Cubison et al., 2005; Good et al., 2010), a dry aerosol sample is mobility size-selected with the first DMA and then humidified to a set RH. The second DMA is then used to measure the size distribution of the humidified aerosol, to give the distribution of growth factor (defined as the ratio of humidified to dry aerosol diameter: D/D_0) as a function of RH and dry diameter ($\text{GF}_{\text{RH}, D_0}$). Quality assurance and inversion of the data was performed using the TDMAinv toolkit of Gysel et al. (2009). During normal operation, the first DMA cycled through five mobility sizes (45, 69, 102, 154, and 269 nm; calibrated values), and the monodisperse flow, after the first DMA, was humidified to a target RH of 90 %. The RH measured in DMA2 remained fairly stable ($\pm 2\%$) for most of the measurement period, and the variation was accounted for by correcting the data to the target RH within the inversion toolkit (Gysel et al., 2009). In addition to this normal mode of operation, humidograms were run on 21 and 23 July. In this mode, cycling through three dry sizes (45, 102, and 269 nm), the RH in the second DMA was gradually varied between 45 and 95 % in order to determine how the GF of ambient aerosol varies with RH.

In both DMAs, a ratio of 10:1 was maintained between the sheath and sample flows, and these were calibrated using an airflow calibrator (Gilibrator-2, Sensidyne). The first DMA was size calibrated at the start of measurements using NIST-traceable polystyrene latex spheres (PSL; Fisher Scientific), sizes 100, 150, 200, and 300 nm, nebulized with an aerosol generator (model ATM 226; TOPAS). Dry scans (in which the sample is not humidified between the DMAs) were run on an approximately weekly basis in order to monitor the size offset between the two DMAs and to define the width of the DMA transfer functions (Gysel et al., 2009). The HT-

DMA was further verified by sampling nebulized ammonium sulfate, monitoring the growth factors for a range of RH (68–92 %) at a given size (140 nm), and comparing to modelled values (ADDEM; Topping et al., 2005). More details of the calibration procedures for this instrument are given by Good et al. (2010).

2.3 CCNc measurements

The CCNc (Roberts and Nenes, 2005) operated downstream of a DMA (model 3081, TSI), the voltage of which was controlled with a classifier (TSI, model 3080), stepping discretely through a mobility size range of 16–325 nm. This quasi-monodisperse aerosol sample flow was then split isokinetically between the CCNc and a CPC (TSI, model 3010). The flow into the CPC was further diluted with filtered air by a factor of 2 in order to match the flow into the CCNc. Inside the CCNc, the aerosol flowed through a wetted column with a temperature gradient, providing supersaturated conditions in which a proportion of the particles activated and were detected by an optical particle counter (OPC) at the bottom of the column. Throughout the deployment, the CCNc cycled through five calibrated supersaturation set points: 0.15, 0.26, 0.47, 0.80, and 1.13 %. The ratio of activated particles to total particles (measured by the CPC) can be determined as a function of dry particle diameter and supersaturation (the activated fraction, AF). By fitting a sigmoid curve function to this activation spectrum, the dry diameter at which 50 % of particles activate (D_{50}) was derived. The hygroscopicity parameter, κ (Petters and Kreidenweis, 2007), was then derived from D_{50} and supersaturation using the κ -Köhler model. In addition, the total number of CCN (N_{CCN}) was calculated by integrating the number size distribution above D_{50} .

The DMA was calibrated using PSLs of the same sizes as with the HTDMA. The CCNc was calibrated by flowing nebulized ammonium sulfate into the system and determining the supersaturation at which 50 % of the particles of a given dry size activate. This critical supersaturation is then compared to modelled values (ADDEM; Topping et al., 2005) to determine the slope and offset.

2.4 Bio-aerosol measurements

Fluorescent biological aerosol particles (FBAPs) in the optical size range of $0.5 \leq D_p \leq 20 \mu\text{m}$ were detected using the WIBS-3M (Kaye et al., 2005; Foot et al., 2008; Stanley et al., 2011), which operates on the principle of ultraviolet-light-induced fluorescence of molecules common to most biological material, specifically tryptophan and the co-enzyme NADH. Two sequential pulses of UV light are provided by filtered Xenon lamps at 280 and 370 nm to excite tryptophan and NADH, respectively. Fluorescence is then detected in the ranges of 310–400 and 400–600 nm following the tryptophan excitation, and 400–600 nm following the NADH excitation (i.e. three fluorescence channels; FL1, FL2, and FL3,

respectively). In addition, the WIBS-3M provides a dimensionless particle asymmetry factor (A_f) as a proxy for particle morphology, as detailed by Crawford et al. (2015). Particles smaller than $0.8 \mu\text{m}$ were rejected from analysis due to low counting efficiency.

The baseline fluorescence of the instrument is measured during so-called forced trigger (FT) sampling periods, where the instrument triggers the flash lamps and records the resultant fluorescence in the absence of aerosol in the sample volume. The mean fluorescence in a FT period is treated as the baseline fluorescence of the optical chamber during the sample period. For a particle to be considered fluorescent (FBAP) it must exhibit a fluorescence greater than a threshold value, defined as the baseline fluorescence plus 3 standard deviations, in any channel. During data processing, the threshold value for each channel is subtracted from the single-particle fluorescence data and the value is clipped at zero with all values greater than zero being considered significantly fluorescent compared to the instrument baseline. All reported fluorescence measurements are relative to the applied threshold and not the absolute detector intensities. This is consistent with previous studies using this instrument (Robinson et al., 2013; Crawford et al., 2014, 2015, 2016), and a detailed description of this data processing method is provided by Crawford et al. (2015). The thresholds remained consistent over 58 FT periods throughout the measurements at 112.4 ± 3.9 for channel FL1, 284.6 ± 7.8 for FL2, and 164.6 ± 5.7 for FL3. The ambient threshold determination method (Perring et al., 2015) was not used here due to the majority of particles being fluorescent in nature.

Size calibration of the WIBS-3M consisted of using PSLs with a physical diameter of $1.0 \mu\text{m}$. Blue fluorescent latex spheres ($1.0 \mu\text{m}$ diameter; Thermo Scientific) were also used to ensure that the excitation and fluorescence channels were operating correctly. The WIBS-3M inlet was operated at a total flow rate of 2.3 L min^{-1} ($\pm 5 \%$). Of this, 90 % was directed through a HEPA filter and used as a sheath flow, constraining the remaining 0.23 L min^{-1} for the scattering chamber sample flow from which particle concentrations were derived.

Particles with fluorescent magnitudes above the threshold are termed FBAPs, as they represent a lower limit of PBAP, some of which may not be detected by this method if their fluorescence goes undetected, or they simply do not fluoresce (Gabey et al., 2010; Huffman et al., 2012). Nonbiological fluorescent material can also be detected by the WIBS should its excitation and emission profile match that of the instrument. Generally, the identified interferents are smaller than the detection limit of the instrument. Polycyclic aromatic hydrocarbons (PAHs), such as naphthalene, and soot-containing PAHs have been shown to fluoresce in FL1 (Pöhlker et al., 2012; Toprak and Schnaiter, 2013); however, they would not be expected to be seen in significant concentrations outside of the pollution events at such a remote site. Mineral dusts contain a small subset of fluorescent aerosol within their popula-

tion ($\approx 10\%$), and given their ubiquitous nature may present a significant source of interferents to the UV-LIF method (Toprak and Schnaiter, 2013). Their observed fluorescent intensity, however, is considerably weaker than is observed for biofluorophores (Pöhlker et al., 2012), and if they were present in any significant concentrations they would likely form their own cluster in the cluster analysis discussed in Sect. 3.4 (Crawford et al., 2016). It should also be noted that the technique does not distinguish between biological particles and fluorescent material attached to nonbiological particles (e.g. dust).

This instrument has previously been deployed in Borneo, and further details of its operation are given by Gabey et al. (2010). In this experiment, the instrument was positioned in a small clearing, a few metres away from the rainforest understorey. It should be noted that the WBS-3M measurements only ran until 10 July, and thus did not overlap with the other principle measurements (HTDMA, CCNc, ACSM) which began on 10 July. Meteorological conditions were fairly consistent over the whole measurement period, and so all measurements discussed here are considered representative of the same general period (i.e. the transition from wet to dry season).

2.5 Removal of pollution episodes

In order to focus on the natural (biogenic) aerosol, for comparison with the wet season, it was necessary to exclude periods affected by pollution. While the site is described as pristine, it can nevertheless be affected by local emissions and regional transport of pollutants: biomass burning emissions from outside the reserve, the urban plume from Manaus, and pollution from the nearby diesel generator.

For each day of the campaign 7-day back trajectories were calculated using the HYSPLIT model (Draxler and Hess, 1998) at 30 min intervals and six altitudes above TT34 (0, 250, 500, 1000, 2000, and 4000 m a.s.l.). The horizontal and vertical wind fields employed here were from the NCEP/NOAA $1^\circ \times 1^\circ$ Global Data Assimilation System (GDAS) reanalysis product. These back trajectories were used to identify air masses arriving at TT34 which had either passed over Manaus or passed nearby active fire zones. The results were largely the same between 0 and 2000 m, with very little influence from the upper-level flow at 4000 m.

A bounding box was drawn between -3.16 and -2.88° latitude and between -60.12 and -59.81° longitude to define the Manaus influence zone (see Fig. 1), and any back trajectory passing over this box at any altitude up to 2000 m was flagged. Air masses potentially impacted by biomass burning were identified by coupling the back trajectory measurements to satellite-detected fires as measured by the MODIS instrument. This operates on the Aqua and Terra satellites, which have local overpass times in the morning and afternoon, respectively. The fire detection data (specific product: MCD14ML) were produced by the University of Mary-

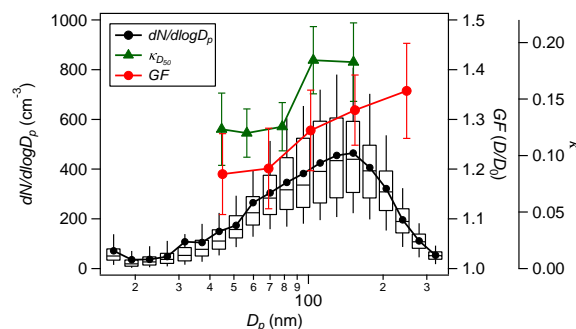


Figure 2. Particle number size distribution averaged over the entire measurement campaign. Box-and-whisker plots show the median, interquartile ranges, and 5th and 95th percentiles, and lines and markers show mean $dN/d\log D_p$. Also shown are κ derived from the D_{50} from the CCNc, and growth factor from the HTDMA, both as a function of particle diameter. Error bars represent ± 1 standard deviation. Note that the HTDMA and CCNc/particle size data have been averaged over slightly different measurement periods, as shown in Figs. 4 and 7.

land and acquired from the online Fire Information for Resource Management System (FIRMS; <https://earthdata.nasa.gov/data/near-real-time-data/firms/about>). At each location along the back trajectories, the surrounding 1° box was interrogated for any fire counts at the nearest Terra/Aqua overpass. If any were present, this trajectory was flagged as potentially influenced by biomass burning. This technique is subject to uncertainties associated with trajectory errors (e.g. Fleming et al., 2012) and the detection of fires in cloudy scenes, or false detection of fires (Schroeder et al., 2008), and therefore can only be considered qualitative. Finally, data were investigated for possible contamination from the generator if the local wind direction was in the range of 270 – 340° ; however, there were no instances of generator contamination during the measurement periods of this study.

In the event of any flag, the black carbon data (from the MAAP) were checked along with the particle counts (where available), and aerosol data were excluded if the pollution flag coincided with a significant increase in these concentrations. No other increases in black carbon concentrations were seen outside the flagged periods. Approximately 28 % of the HTDMA and CCNc data were removed in this way, with 5 % of the data being flagged as possibly impacted by biomass burning and most of the rest removed due to the Manaus urban plume. The ACSM, which was not necessarily operating at the same times as the HTDMA and CCNc, had approximately 9 % of its data removed due to pollution flags (almost entirely due to the urban plume from Manaus).

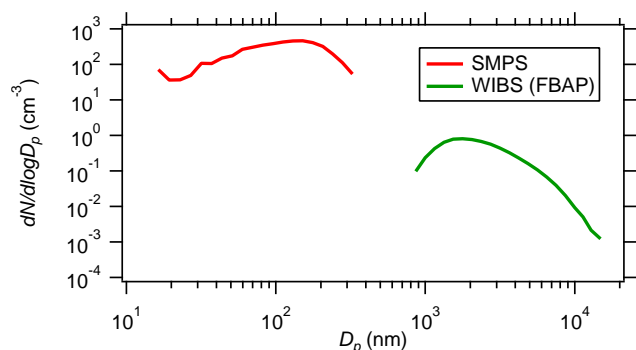


Figure 3. Combined log–log plot of total particle number size distribution (as measured with the SMPS) with FBAP number size distribution (from the WIBS). It should be noted that the SMPS measured the mobility diameters of particles in a dried sample, while the WIBS measured optical diameters at ambient humidity.

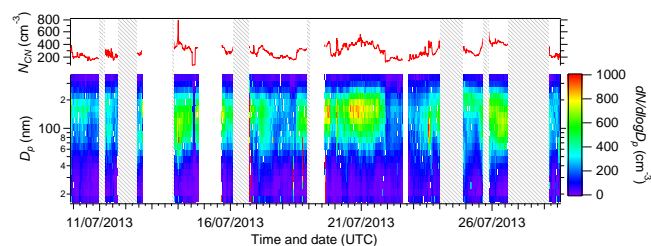


Figure 4. The time series of total particle counts (integrated from size distributions; top panel) and particle number size distribution (bottom panel). Shaded areas represent pollution episodes removed from the data. Any other gaps are due to instrument downtime.

3 Results and discussion

3.1 Size distributions

The particle number size distribution recorded over the measurement period of this study can be seen in Fig. 2. This shows a broad accumulation-mode peak at 130–150 nm with a median number concentration of 266 cm^{-3} (calculated from the integral of the size distribution curve). Despite observing aerosol number concentrations comparable to previous observations during the wet season, the shape of the distribution resembles those measured in the dry season, although the concentrations during the latter are considerably higher at 2200 cm^{-3} (Artaxo et al., 2013). Figure 3 shows the size distribution again combined with the coarse-mode FBAP measurements from the WIBS. In terms of number concentration, the submicron modes dominate the coarse mode by a factor of 10^3 . The WIBS measurements are discussed in further detail below.

The size distribution, however, was quite variable over the period of the measurements, as can be seen in the time series in Fig. 4, and varied with total particle number concentrations. Median size distributions observed when the to-

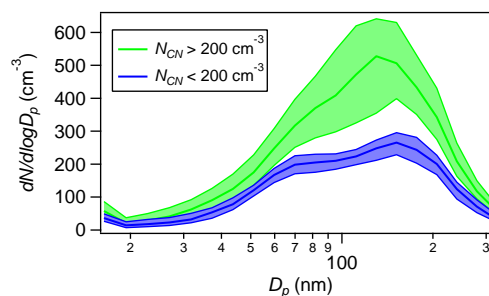


Figure 5. Median and interquartile ranges of particle number size distributions observed during high ($> 200 \text{ cm}^{-3}$) and low ($< 200 \text{ cm}^{-3}$) total particle number concentrations.

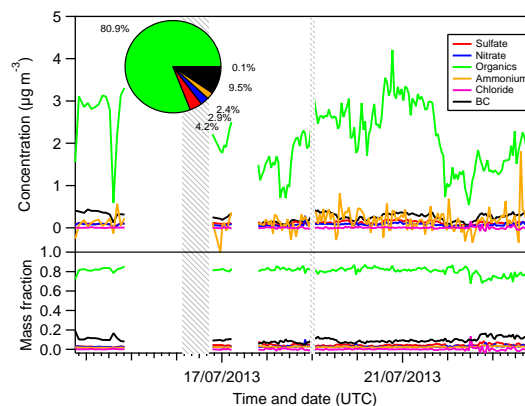


Figure 6. Submicron nonrefractory aerosol composition from the ACSM measurements along with equivalent black carbon from the MAAP measurements: concentration (top panel) and mass fraction (bottom panel). The pie chart shows the average proportions over the measurements. Shaded areas represent pollution episodes removed from the data. Any other gaps are due to instrument downtime.

tal number concentration was above or below 200 cm^{-3} are shown in Fig. 5. During periods of low particle counts, an Aitken mode is also seen, with a mode around 80 nm, while the size distribution during episodes of higher concentrations is dominated by the accumulation mode, possibly masking the smaller mode. Such a size distribution profile, dominated by accumulation-mode aerosols, has also been reported during the dry season in western Amazonia, in the deforestation arc, during biomass burning events (Brito et al., 2014), albeit with substantially higher concentrations.

3.2 Composition

Submicron nonrefractory aerosol composition, as measured by the ACSM during the period of this study, is illustrated in Fig. 6. The mean mass loadings for organic material, sulfate, and nitrate were 2.13 ± 0.75 , 0.11 ± 0.04 , and $0.08 \pm 0.03 \mu\text{g m}^{-3}$, respectively (± 1 standard deviation). Organic material dominated the submicron aerosol, comprising

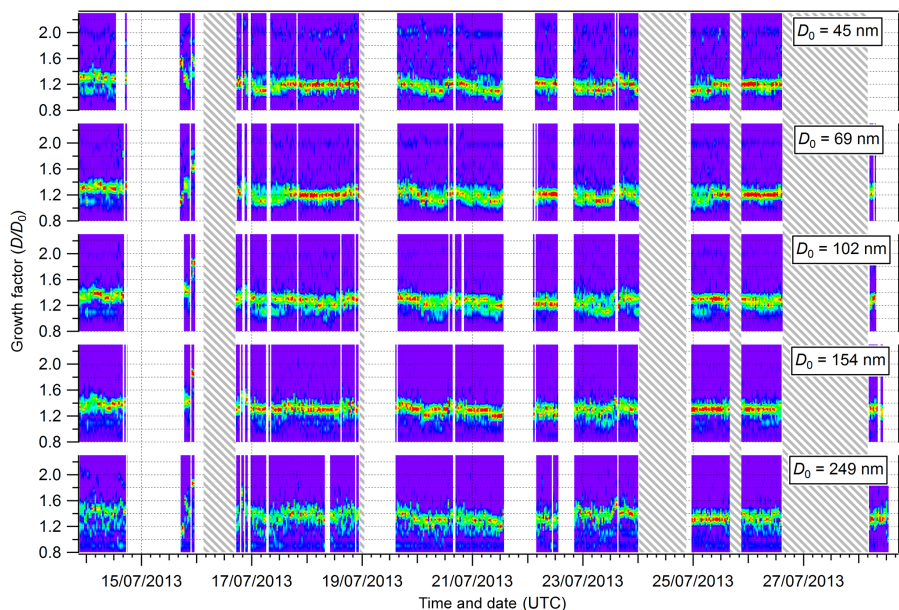


Figure 7. The time series of normalized RH-corrected (to 90 %) growth factor distributions derived from HTDMA measurements, for all five dry diameters. Shaded areas represent pollution episodes removed from the data. Any other gaps are due to instrument downtime and humidograms.

around 81 % of the total mass (86 % of nonrefractory material), on average. Such a high fraction of organics compares well with previous observations in the Amazon basin (Artaxo et al., 2013; Brito et al., 2014; Andreae et al., 2015). BC_e concentrations are also shown, with a mean mass loading of $0.25 \pm 0.01 \mu\text{g m}^{-3}$. This is consistent with previous wet season measurements in the Amazon (Artaxo et al., 2013; Andreae et al., 2015).

The mass fractions of nonrefractory aerosol and BC_e are shown in the bottom panel of Fig. 6. Due to the noise in the ammonium signal (see Fig. 6), resulting from concentrations below the limit of detection of $0.3 \mu\text{g m}^{-3}$ for the ACSM, it was necessary to estimate the ammonium from the nitrate and sulfate mass loadings for the purpose of mass fraction calculations. The time series of mass fractions show that, while the mass loadings vary considerably, particularly in organics, the composition is relatively consistent as a proportion of the aerosol mass. Organic mass fractions remain steady around 81 % of the total mass, until 22 and 23 July, when a slight increase in BC_e is seen.

Levoglucosan, a major constituent of biomass burning aerosol, fragments in AMS and ACSM instruments at a mass-to-charge ratio (m/z) of 60 (Alfarra et al., 2007), and so the fraction f_{60} is frequently used as a marker for biomass burning (Artaxo et al., 2013; Chen et al., 2009). The mean f_{60} from the ACSM data in this study, after removal of pollution episodes, was $0.19 \pm 0.07 \%$. This is well below 0.3 %, which is considered to be the upper limit for background air masses not affected by biomass burning (Cubison et al., 2011). It should be noted that previous studies in the Amazon

have observed that a large fraction of the biomass-burning related organic aerosols do not present a significant f_{60} signal, due to long-range transport (BrITO et al., 2014). It can be said, however, that the relatively low f_{60} observed here suggests that, on average, these measurements were not strongly impacted by local biomass burning emissions.

Previous studies have successfully identified FBAP markers on ambient aerosol in the Amazon using an aerosol mass spectrometer (Schneider et al., 2011), a method which relies strongly on the high-resolution capabilities of the instrument used at the time. Given the unity mass resolution of the ACSM, similar methodology has not been applied here.

3.3 Aerosol water uptake

The HTDMA ran from 13 to 28 July. Figure 7 shows the time series of RH-corrected GF distributions for all dry sizes, as derived from the HTDMA data using the TDMAinv toolkit. These largely exhibit a single mode at each size, roughly in the range of 1.2–1.4. Some variability can be seen, for example on 21 and 23 July, but for the most part, peak growth factors remained relatively stable over the measurement period. This is consistent with the stable mass fractions seen in the composition data from the ACSM (see Fig. 6, bottom panel). The variability and slight decrease in GF at some sizes on 22 and 23 July may also be attributed to the slight increase in the mass fraction of BC_e (Fig. 6). High peak growth factors (> 1.6) can briefly be seen on the night of 15 July, shortly before a pollution event; however, without composition data

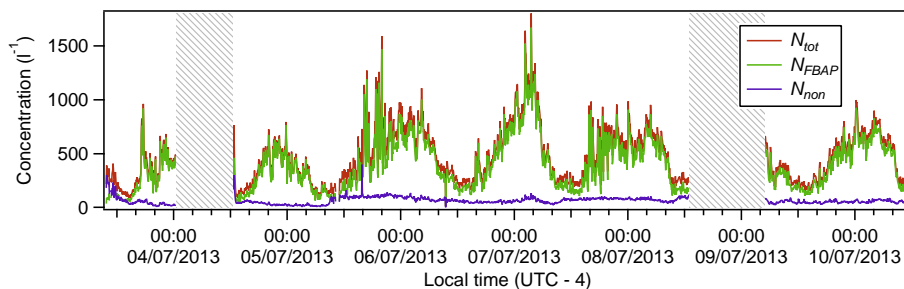


Figure 8. The time series of total, FBAP, and non-FBAP number concentrations, as measured by the WIBS-3M. Shaded areas represent pollution episodes removed from the data. Any other gaps are due to instrument downtime.

Table 1. Mean peak growth factors and derived κ from HTDMA measurements for each dry diameter, along with \pm standard deviation.

D_0 (nm)	GF	κ
45	1.19 ± 0.08	0.09 ± 0.10
69	1.20 ± 0.08	0.09 ± 0.09
102	1.28 ± 0.08	0.12 ± 0.10
154	1.32 ± 0.07	0.15 ± 0.09
249	1.36 ± 0.10	0.17 ± 0.09

Table 2. Mean derived parameters from CCNc measurements for each set supersaturation (SS), along with \pm standard deviation.

SS (%)	D_{50} (nm)	κ	N_{CCN} (cm $^{-3}$)
0.15	152 ± 9.5	0.18 ± 0.03	87 ± 35
0.26	105 ± 5.5	0.18 ± 0.03	161 ± 60
0.47	78 ± 4.2	0.13 ± 0.02	212 ± 74
0.80	56 ± 3.0	0.12 ± 0.02	248 ± 82
1.13	45 ± 3.4	0.12 ± 0.03	268 ± 86

available on that day (Fig. 6), it is difficult to speculate as to the nature of this.

Smaller, more hygroscopic ($GF > 1.5$) modes can be seen at the lower dry diameters, while the larger particles also show a hydrophobic mode in the growth factor distribution. The contribution of the hydrophobic mode to the larger particles is small ($< 10\%$ in number) and may be due to some unknown local anthropogenic influence that was not accounted for. The averages of the growth factor at the peak of the growth factor distribution (i.e. the dominant mode) are shown in Table 1 and Fig. 2. They show an increase with dry diameter, reflecting the difference between Aitken- and accumulation-mode aerosol: organic mass fractions are highest in the Aitken mode, while elevated sulfate mass fractions have been previously seen in the accumulation mode (Gunthe et al., 2009; Pöschl et al., 2010). It should be noted, however, that the elevated sulfate events observed by Gunthe et al. (2009) were likely linked to long-range transport of biomass

burning aerosol from Africa, which, due to a combination the African burning season and large-scale circulation, tends to impact the Amazon forest more often during the wet season (Ben-Ami et al., 2010).

The campaign averages of the CCNc-derived parameters, D_{50} , κ , and N_{CCN} are given for each set supersaturation in Table 2. The κ values are also plotted against D_{50} in Fig. 2. Consistent with the growth factor data, and with previous measurements at this site (Gunthe et al., 2009), they show more hygroscopic particles at larger diameters ($\kappa \approx 0.12$ below 100 nm, and $\kappa \approx 0.18$ around the accumulation mode).

Reconciliation between subsaturated and supersaturated particle water uptake for these measurements has already been investigated by Whitehead et al. (2014). They showed that there was agreement within the variability of the data, with a slightly underestimated hygroscopicity from the HTDMA data compared to the CCNc at lower supersaturations (larger dry diameters). The analysis of Whitehead et al. (2014) considered the full data set without separating out the pollution events; however, performing the same analysis on the clean data did not result in any significant difference.

3.4 FBAP measurements

Measurements of biological particles in the Amazon are important as they are considered to have a strong influence on clouds as ice nuclei (Pöschl et al., 2010). The WIBS-3M operated uninterrupted from the morning of 3 July to 10 July. The mean particle number concentration measured by the WIBS-3M during this period was $464 \pm 250 \text{ L}^{-1}$ (1 standard deviation), while the mean FBAP number concentration was $400 \pm 242 \text{ L}^{-1}$ (i.e. accounting for 86 % of the particles in the size range of the instrument). The time series of number concentrations for the duration of this period is shown in Fig. 8. This shows coarse-mode particles were dominated by FBAP number concentrations, which exhibited a strong diurnal cycle with concentrations varying from around 200 L^{-1} during the daytime up to as much as 1200 L^{-1} at night. The diurnal variation (Fig. 9) shows that FBAP number concentrations plateaued from around 21:00 through the night, began to drop from 05:00, reached a minimum by 11:00 and started

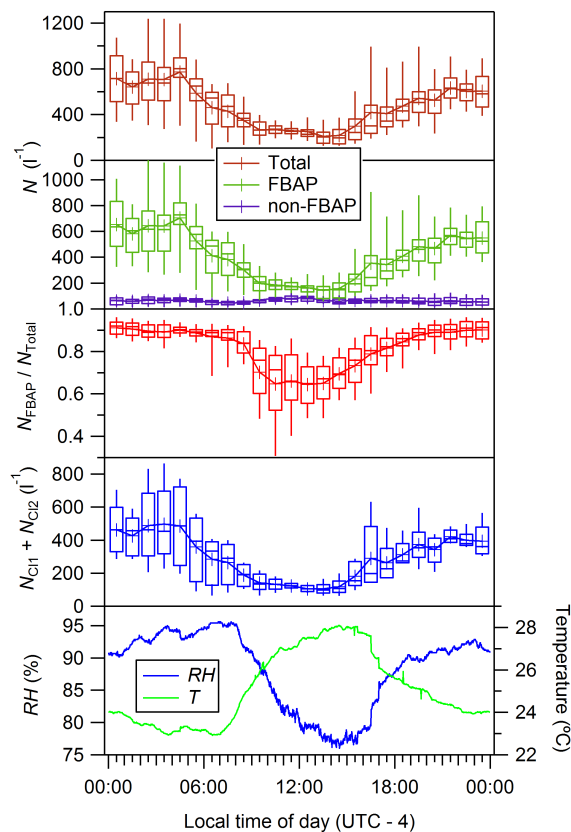


Figure 9. Diurnal variations in total, FBAP, and non-FBAP number concentrations, as measured by the WIBS-3M, as well as the fraction of FBAPs, and the combined number concentrations of clusters C11 and C12. Shown are the means (lines and markers), medians and interquartile ranges (boxes), and 5th and 95th percentiles (whiskers). Also shown at the bottom are the mean diurnal variations in temperature and RH, measured on the tower above the canopy, for the same period.

increasing again from 15:00. The FBAP fraction was highest (more than 90 %) at night, and remained high until around 08:00 – even after FBAP number concentrations began decreasing. This dropped to between 55 and 75 % during the day, helped in part by an apparent increase in non-FBAP concentrations, before steadily increasing in line with the FBAP concentrations through the late afternoon/early evening.

There are a number of factors driving the diurnal cycle in coarse-mode particles, as discussed by Huffman et al. (2012). Previous studies at this and a nearby site, utilizing electron and light microscopy, have identified the FBAPs as predominantly fungal spores (Graham, 2003; Huffman et al., 2012). Similar diurnal cycles have been seen in airborne fungal spore densities at other tropical rainforest locations (Gilbert and Reynolds, 2005; Elbert et al., 2007). The observed nighttime peak in FBAP number concentrations in Fig. 9 is consistent with nocturnal sporulation driven by increasing RH (see bottom panel; note that RH is measured above the canopy).

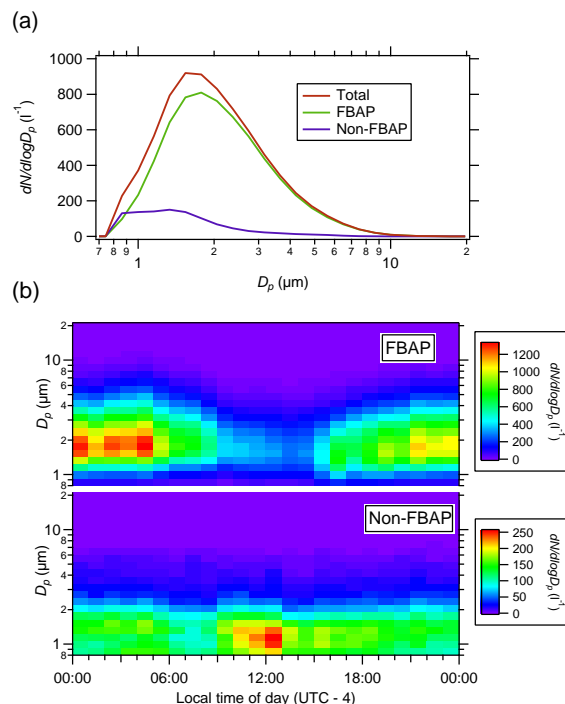


Figure 10. Particle number size distributions measured with the WIBS-3: (a) mean size distributions for total, FBAPs, and non-FBAPs; and (b) diurnal variation of size distribution for FBAPs and non-FBAPs (note that the colour scales are not the same).

The dependence of fungal spore release on meteorological conditions, however, varies greatly according to species, and any relationship is nontrivial (Jones and Harrison, 2004). FBAP number concentrations begin dropping several hours before any decrease in RH, and the FBAP fraction also remains high (Fig. 9). This suggests that the morning decrease in FBAPs is not necessarily due to a cessation of emission processes, but may also be the result of a breakup of the nocturnal boundary layer around sunrise (Whitehead et al., 2010; Huffman et al., 2012). Graham (2003) and Huffman et al. (2012) suggest that the nighttime increase in coarse-mode particles is due, at least in part, to the shallow nocturnal boundary layer. The slight increase in non-FBAP concentrations during the day may be a result of enhanced particle exchange through the canopy, facilitated by sporadic turbulent events, as described by Whitehead et al. (2010), bringing non-FBAPs that had originated elsewhere into the space below canopy.

Figure 10 shows the number size distributions reported by the WIBS-3M during the measurement period. Again, FBAPs clearly dominate the particle number concentrations for $D_p > 1 \mu\text{m}$; however, non-FBAP concentrations are higher for particles smaller than $1 \mu\text{m}$ measured by the WIBS-3M (i.e. down to the instruments 50 % detection diameter of $0.8 \mu\text{m}$). The FBAP number size distribution shows a peak at around $1.8 \mu\text{m}$, while the non-FBAP distribution

Table 3. Solutions to the Ward linkage cluster analysis, showing mean (± 1 standard deviation) intensity in each fluorescence channel (FL1–3), optical particle diameter (D_p), and asymmetry factor (A_f). The intensities are referenced to the FT + 3 standard deviation threshold representing an intensity of zero, as discussed in Sect. 2.5. Fluorescent intensities and asymmetry factors are in arbitrary units.

	C11	C12	C13
FL1 (280 nm)	1400 \pm 302	478 \pm 386	386 \pm 533
FL2 (280 nm)	120 \pm 96	33 \pm 47	351 \pm 212
FL3 (370 nm)	94 \pm 106	47 \pm 73	721 \pm 379
D_p (μm)	2.5 \pm 1.3	1.9 \pm 1.0	2.3 \pm 1.1
A_f	30.9 \pm 15.0	30.2 \pm 15.7	29.0 \pm 15.1

is characterized by a flatter, broader peak between 0.8 and 1.3 μm . Nonfluorescent particles at this site have previously been identified as mineral dust, nonfluorescent biological aerosol, and inorganic salts (Huffman et al., 2012). Caution must be applied when interpreting the submicron fluorescent aerosol fraction due to the reduced fluorescent counting efficiency for particles $D_p < 0.8 \mu\text{m}$ (Gabey et al., 2011), which may lead to an underestimation of the fluorescent aerosol fraction at small sizes.

A Ward linkage cluster analysis using the z score normalization was applied to the data, where the optimum number of retained distinct clusters was determined using the Calinski–Harabasz criterion. Prior to analysis, all nonfluorescent and saturated particles, and particles smaller than 0.8 μm in diameter were excluded, resulting in approximately 15 % of the single-particle data being rejected. The asymmetry factor and size inputs were converted to log space prior to normalization and clustering. Complete information on this technique is given by Crawford et al. (2015), who used the same instrument model in the same way as in this study. This analysis revealed three distinct fluorescent classes of particles (C11–3). The statistical parameters of each cluster are shown in Table 3. It can be seen that C11 and C12 display similar characteristics; specifically, they mainly fluoresce in FL1 with weak fluorescence in the other channels, although the intensities are greater for C11, suggesting they are distinct subclasses. The two clusters correlate strongly ($r^2 = 0.86$) with each other; hence, both have been combined in Fig. 9. They show similar fluorescent signatures to the clusters attributed to fungal spores by Crawford et al. (2014, 2015) based on comparison with other sampling techniques and the diurnal emission pattern. In this study, they show higher concentration overnight (Fig. 9), and a strong correlation to RH (Fig. 11). Together, clusters C11 and C12 contribute approximately 70 % to the total fluorescent particle concentration, regardless of time of day, suggesting that FBAPs were dominated by fungal spores during this study. A third cluster, C13, shows very low concentrations (around 20 L^{-1}), with no strong diurnal trend; however, there are insufficient data to speculate upon the nature of this cluster (such as response to

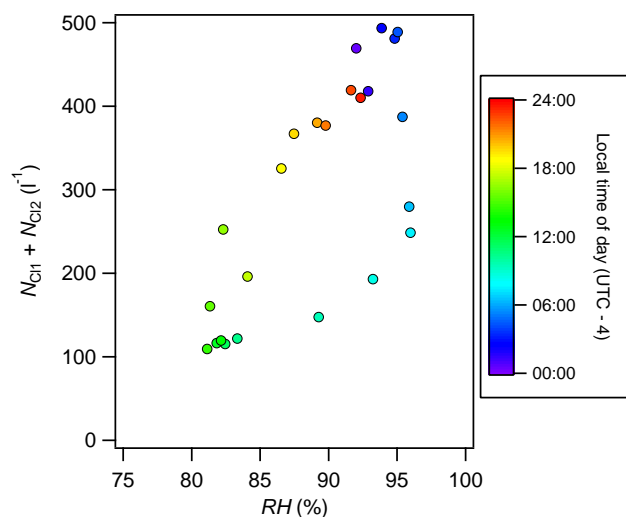


Figure 11. Diurnal means of total particle number concentrations in clusters 1 and 2, plotted against RH.

rainfall). The asymmetry factor for each cluster was around 30, suggesting that the particles are aspherical in nature. A similar value of asymmetry factor was observed by Crawford et al. (2015) in the ambient fungal cluster, further suggesting that clusters C11 and C12 are representative of fungal spores.

PBAP classification via the comparison of single-particle fluorescent signatures to laboratory samples is an ongoing area of research (e.g. Hernandez et al., 2016). Such direct comparison for this purpose is not possible here due to differences in the instruments used (i.e. different excitation/detection wavebands and optical chamber design). Even comparing results between the same model of instrument with identical detector/filter configurations has been difficult (Hernandez et al., 2016) due to the current lack of a robust fluorescence calibration method.

3.5 Comparison with previous studies

3.5.1 Submicron aerosol

Aerosol water uptake studies have previously been conducted at the TT34 site by Gunthe et al. (2009) using size-selected CCNc measurements, and at Balbina (110 km NE of TT34) by Zhou et al. (2002) using a HTDMA, both during the wet season. HTDMA and CCNc measurements were also made at Balbina during the transition from wet to dry season by Rissler et al. (2004). In addition, HTDMA measurements from pasture land in southwest Amazonia at the end of the dry season/beginning of wet season are presented by Rissler et al. (2006) and Vestin et al. (2007). This study represents the first measurements with HTDMA and monodisperse CCN instruments at TT34 during the transition from wet to dry seasons. Concurrent CCNc and HTDMA measurements have also been conducted in Borneo, southeast Asia,

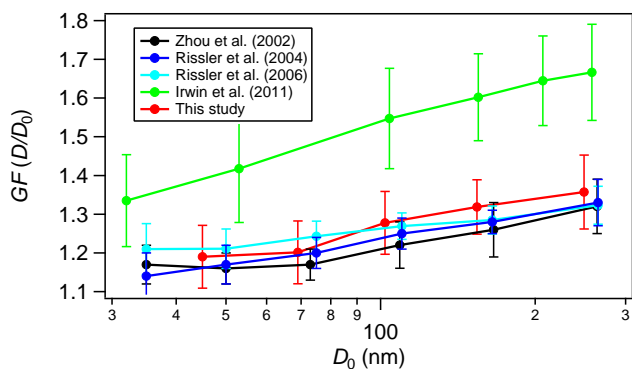


Figure 12. Mean growth factor for the dominant, less hygroscopic mode plotted against dry diameter, comparing this to previous studies in Amazonia and Borneo. The data from Rissler et al. (2004) and Rissler et al. (2006) represent less hygroscopic and moderately hygroscopic particles (respectively) during the wet season. The definitions differ slightly between the studies in terms of GF range, but the modes represented here broadly fit into the less hygroscopic classification of Swietlicki et al. (2008). Error bars represent ± 1 standard deviation.

by Irwin et al. (2011), providing a useful comparison with a different tropical rainforest region.

The HTDMA growth factor measurements of Zhou et al. (2002) showed a similar pattern to this study: a dominant mode of less hygroscopic particles ($GF \approx 1.16$ – 1.32), accompanied at times by a hydrophobic mode ($GF < 1.06$; particularly at the larger particle sizes), and a more hygroscopic mode ($GF \approx 1.38$ – 1.54). The growth factors of the less hygroscopic particles are compared in Fig. 12, along with the other studies (note that Rissler et al. (2004) define “less hygroscopic” as $GF \approx 1.17$ – 1.5). All the measurements showed a similar increase in growth factor with dry diameter. The growth factor values from this study were slightly higher than those of Zhou et al. (2002) and Rissler et al. (2004), but the difference is within the variability of the measurements, and probably within the variability that has been seen between different HTDMA instruments (Duplissy et al., 2009; Massling et al., 2011). The moderately hygroscopic particles ($GF = 1.26$) observed by Rissler et al. (2006) exhibited growth factors in the same range as the other studies in Amazonia; however, in this case, the hydrophobic mode ($GF \approx 1.05$ – 1.13) was dominant for all but the larger particles (> 135 nm). Furthermore, strong diurnal cycles (daytime increases in the fraction of moderately hygroscopic particles) were observed (Rissler et al., 2006; Vestin et al., 2007), which were not seen during the current study. In contrast to the current study, the measurements of Rissler et al. (2006) and Vestin et al. (2007) were conducted in a region that has undergone heavy land use change and is strongly influenced by anthropogenic sources (Andreae et al., 2002), which may contribute to the observed diurnal pattern.

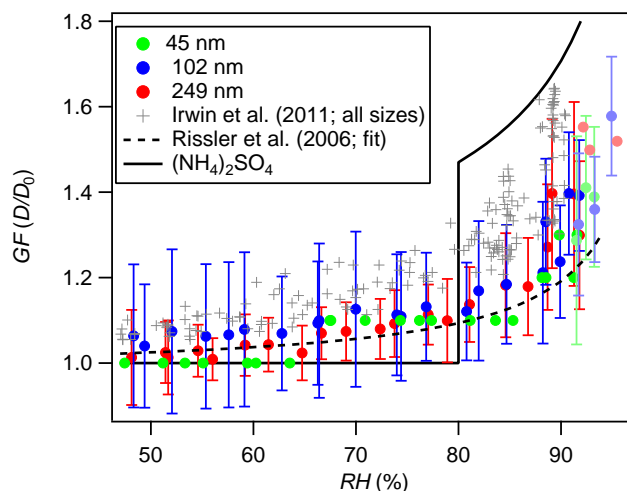


Figure 13. Humidogram (dependency of growth factor on RH), taken between 14:00 and 20:30 UTC on 21 July. The fainter points at higher RH were taken between 13:30 and 14:30 UTC on 23 July. The humidogram data from Irwin et al. (2011), and the humidogram fit from Rissler et al. (2006) are also shown, for comparison. The black line shows the modelled humidogram for ammonium sulfate (Topping et al., 2005) for reference.

In contrast to the studies from Amazonia, aerosol growth factors measured in Borneo (Irwin et al., 2011) were somewhat higher, in the range of 1.3–1.7 (Fig. 12). This can be explained by the fact that, while the site in the Amazon benefited from a fetch of hundreds of kilometres of undisturbed rainforest, the site in Borneo was heavily influenced by marine air masses (Robinson et al., 2011). As discussed by Robinson et al. (2011), the sulfate loadings in Borneo were substantially higher than in Amazonia, even in air masses from across the island, which, with sulfate being more hygroscopic than organic aerosol, is a possible explanation for the higher growth factors.

The results of the humidogram are shown in Fig. 13, and compared to the humidogram data from Borneo (Irwin et al., 2011) and the humidogram fit for the wet season data of Rissler et al. (2006). Growth factors in Borneo were higher across the RH range than in Amazonia. As with previous measurements, no deliquescence behaviour was seen in this study.

Values of κ derived from the HTDMA and CCNc measurements during these studies are compared in Fig. 14, as a function of dry diameter. Here, the κ from HTDMA measurements is derived using the average growth factor, rather than the peak of the less hygroscopic mode, for direct comparison with the CCNc-derived values. The various measurements in Amazonia showed very similar κ , largely agreeing within the variability of the individual measurements. It can be said that water uptake measurements in Amazonia are consistent, and, as noted by Gunthe et al. (2009), show κ to be around half

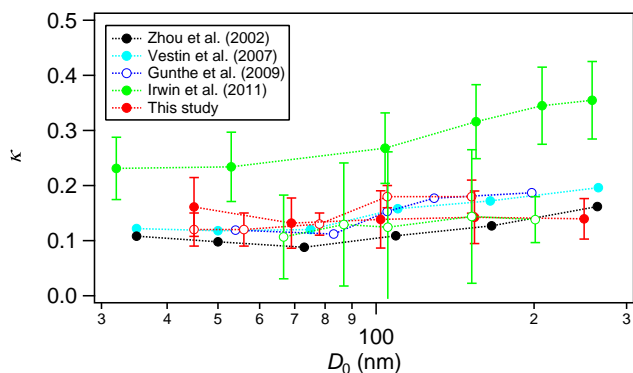


Figure 14. Comparing κ as a function of diameter for this and previous studies in Amazonia and Borneo. Filled circles represent HTDMA-derived values, while empty circles are CCNc-derived values. Error bars represent ± 1 standard deviation, where these data are available. The values for Zhou et al. (2002) and Vestin et al. (2007) were calculated by Gunthe et al. (2009).

that typically seen in other continental regions (Andreae and Rosenfeld, 2008).

The HTDMA-derived κ from the Borneo experiment shows more hygroscopic aerosol than in Amazonia, as discussed above; however, the CCNc-derived values are more in line with those in Amazonia. This discrepancy has been noted previously and possible reasons for it are discussed by Irwin et al. (2011) and Whitehead et al. (2014). These were mainly related to differences in the instrument setups and how they treat the aerosol. It should be noted that the discrepancy in the data from the Borneo experiment was the largest amongst a number of data sets studied by Whitehead et al. (2014), but the reason for this is not clearly understood.

In general, the particle concentrations and hygroscopic properties observed during this study were similar to those seen during wet season measurements in the Amazon rainforest. The main difference seen was that size distributions in this study were more strongly dominated by the accumulation mode: similar to those seen in the dry season (Artaxo et al., 2013), but in clean conditions with significantly lower number concentrations. Under these conditions, cloud droplet formation in convective clouds in this region is likely to be aerosol limited (Reutter et al., 2009). Previous modelling studies have suggested this is the case during the wet season (Pöschl et al., 2010), in contrast to the dry season during periods of intense biomass burning when droplet number is largely controlled by the updraft velocity (Reutter et al., 2009).

In terms of composition, submicron nonrefractory aerosol concentration during this experiment showed significantly higher concentration ($\approx 2.5 \mu\text{g m}^{-3}$) than observed at the remote sites in central Amazonia in previous years during the wet season, ranging from $0.4 \mu\text{g m}^{-3}$ (Artaxo et al., 2013) to $0.6 \mu\text{g m}^{-3}$ (Chen et al., 2009; Andreae et al., 2015). Conversely, the concentration is significantly lower than reported

during the dry season ($8.9 \mu\text{g m}^{-3}$) (Andreae et al., 2015), due to this transitional period having no extensive biomass burning activities, albeit with already reduced wet deposition due to reduced precipitation. Interestingly, despite the marked changes in ambient concentration, very little difference is observed in terms of relative contributions considering this and previous studies, being strongly dominated by organics ($\approx 80\%$), followed by sulfate and minor contribution of nitrate and ammonium (Chen et al., 2009; Artaxo et al., 2013; Andreae et al., 2015).

It is not clear how meteorological conditions influence the differences between this study and those in the wet season. The warmer, dryer conditions of this study might result in more evaporation of SOA, whereas more precipitation in the wet season would lead to more washout, and therefore lower loadings. From the results, it would seem that the latter effect dominates, resulting in the higher organic loadings and accumulation-mode aerosol seen in this study, but there may be other, more complex factors. Long-term measurements would be needed to fully investigate the influence of meteorology on particles in the Amazon.

3.5.2 Coarse-mode aerosol

Huffman et al. (2012) conducted measurements of FBAPs at the TT34 tower using an ultraviolet aerodynamic particle sizer (UV-APS) during the AMAZE-08 campaign. In contrast to this study, the AMAZE-08 measurements were taken during the wet season (February–March) from the top of the tower (i.e. above canopy). It is also worth comparing with the measurements of Gabey et al. (2010), who used the same WIBS-3 instrument to sample the aerosol above and below canopy in the rainforest of northeast Borneo.

The median number concentration of FBAP observed below the canopy in the current study was 363 L^{-1} , while the UV-APS measurements at the top of the tower by Huffman et al. (2012) were around a fifth of this at 73 L^{-1} (also median). In an intercomparison between the two different measurement techniques, Healy et al. (2014) found that, while there was agreement in total number concentrations, the counts in the fluorescence channels of the WIBS (particularly FL1) were substantially higher than the UV-APS fluorescence counts, which would at least partly explain the difference here. The wetter, more humid conditions during the wet season measurement period of Huffman et al. (2012) would be expected to favour emission (Jones and Harrison, 2004; Zhang et al., 2015). On the other hand, the higher rainfall would also result in enhanced wet deposition during the wet season, especially above canopy. At other locations, Gabey et al. (2010) saw concentrations in Borneo often in excess of 1500 L^{-1} below canopy and around 200 L^{-1} above, using the same instrument at each site, while Gilbert and Reynolds (2005) observed substantially higher concentrations of fungal spores in the understorey than in the canopy during measurements in Queensland, Australia. Strong vertical gradients

in biological particles are therefore regularly seen in rainforest environments, and would be an additional factor in the differences observed between the measurements at TT34. In a remote tropical rainforest in China, Zhang et al. (2015) estimated fungal spore concentrations to be around 50 L^{-1} based on chemical analysis of filters, and found higher concentrations associated with rainfall events. A global modelling study by Spracklen and Heald (2014) found simulated surface annual mean concentrations of fungal spores to be around 100 L^{-1} over tropical forests (including central Amazonia), which is consistent with this and other measurements at this site.

The fraction of FBAPs in this study was, on average, 85 % of total coarse-mode particles (and as much as 90 %), whereas it was 24 % in the AMAZE-08 campaign (41 % in unpolluted conditions). The higher fraction at ground level would be expected, being closer to the source, whereas above canopy there is a stronger influence from nonfluorescent particles from external sources. Elbert et al. (2007) found fungal spores accounted for 35 % of coarse-mode particles, also in central Amazonia, but their filter samples were taken at a pasture site adjacent to the rainforest. In Borneo, as in the Amazon, there was a higher fraction below the canopy (55 %) than above (28 %), however not as high as the 86 % observed in this study. Reasons for this difference are unclear, but may include a stronger influence in Borneo of nonfluorescent particles from external sources, such as the nearby coast. More consistent with the current study were the scanning electron microscopy (SEM) measurements reported by Pöschl et al. (2010) and Huffman et al. (2012), which attributed 80 % of coarse-mode particles to primary biological aerosol during the AMAZE-08 campaign, and also identified particles likely to be fungal spores.

One difference between the measurements of this study and others is the position of the mode in the FBAP number size distribution. Gabey et al. (2010) report the peak at $2.5 \mu\text{m}$, while Huffman et al. (2012) observe the peak around $2.3 \mu\text{m}$. By contrast, the peak in this study was $1.8 \mu\text{m}$. The difference between the two measurements at TT34 is likely due to the different measurement techniques, with the UV-APS found to be less sensitive to smaller fluorescent particles (Healy et al., 2014).

Diurnal variations between this study and that of Huffman et al. (2012) were similar; however, Gabey et al. (2010) reported an additional increase in FBAP number concentrations in the afternoon in Borneo. This increase coincided with a peak in RH, and it is believed that this is linked (Gabey et al., 2010). In this study, the RH increased more gradually through the afternoon and evening (see Fig. 9, bottom panel), which may explain the lack of afternoon peak in FBAPs compared to the Borneo results. Huffman et al. (2012) also do not observe a mid-afternoon peak in FBAPs.

4 Conclusions

Measurements of aerosol concentrations and water uptake properties were conducted at a remote site in pristine Amazonian rainforest in July 2013, during the transition from the wet to dry season. Back trajectories and wind sectors were examined in conjunction with black carbon concentrations in order to exclude any pollution episodes and ensure the aerosols measured were representative of background aerosol over the rainforest.

With any pollution episodes removed from the data, particle concentrations were low, with a median of 266 cm^{-3} . The particle size distributions were largely dominated by an accumulation mode around 130–150 nm, with a smaller Aitken mode apparent during periods of lower particle counts. Based on previous measurements contrasting wet and dry seasons (Artaxo et al., 2013), the results here may reflect the transition between the two seasons, with periods consistent with each at different times (but without considering any influence from biomass burning).

Aerosol chemical composition, as measured with an ACSM, was dominated by organic material, comprising around 81 % of the total mass of nonrefractory aerosol and BC_e . The mass fraction of organics was relatively consistent over the measurement period.

Aerosol water uptake and hygroscopicity was measured using an HTDMA and a CCNc. Good agreement was found between the measurements of both instruments. Particle growth factors from the HTDMA varied little over most of the measurement period and were typically between 1.2 and 1.4 (low hygroscopicity mode). Aerosol hygroscopicity was found to be low ($\kappa = 0.12$) for Aitken-mode particles, and increased slightly to $\kappa = 0.18$ for accumulation-mode particles. This is consistent with previous measurements at or near this site, and with the observation that Aitken-mode particle composition is dominated by organic material, while accumulation-mode particles exhibited higher sulfate mass fractions (Pöschl et al., 2010).

Particles in the size range of $0.5 \leq D_p \leq 20 \mu\text{m}$ were measured using the WIBS-3M, which distinguishes fluorescent (representing a subset of primary biological aerosols, or FBAPs) and nonfluorescent particles. FBAPs dominated the coarse-mode aerosol, accounting for as much as 90 %. Concentrations of FBAPs followed a strong diurnal cycle, with maximum concentrations during the night. This is likely driven by a combination of the dependence of emission processes on meteorological conditions and the diurnal cycle of the boundary layer.

The results from this study were also compared to measurements conducted in Borneo in 2008 (Irwin et al., 2011; Gabey et al., 2010; Robinson et al., 2011), contrasting the vast green ocean of the Amazon rainforest to the island rainforest geography of southeast Asia. In the submicron range, aerosol hygroscopicity was greater in Borneo, possibly due to the stronger marine influence of that region (Irwin et al.,

2011). Coarse-mode particles at both locations were dominated by FBAPs (probably mostly fungal spores). Below canopy, the Amazon exhibited a higher fraction of FBAPs than Borneo, though higher FBAP concentrations were seen at the latter.

5 Data availability

The data published here will shortly be made available on the Centre for Environmental Data Analysis – Atmospheric Science (CEDA-AS; <http://www.ceda.ac.uk/>). In the meantime, any requests for data can be made to the corresponding author, Gordon McFiggans (g.mcfiggans@manchester.ac.uk).

Acknowledgements. The authors wish to thank the Large-scale Biosphere-Atmosphere (LBA) project group at the National Institute for Amazonian Research (INPA) in Manaus for logistical support before and during the field deployment. The Brazil–UK Network for Investigation of Amazonian Atmospheric Composition and Impacts on Climate project was funded by the UK Natural Environment Research Council (NERC; grant NE/I030178/1). NERC also funded the PhD studentship of E. Darbyshire. J. Brito was funded by Fundação de Amparo à Pesquisa do Estado de São Paulo (FAPESP; project 2013/25058-1).

Edited by: A. Huffman

Reviewed by: three anonymous referees

References

- Alfarra, M. R., Prevot, A. S. H., Szidat, S., Sandradewi, J., Weimer, S., Lanz, V. A., Schreiber, D., Mohr, M., and Baltensperger, U.: Identification of the Mass Spectral Signature of Organic Aerosols from Wood Burning Emissions, *Environ. Sci. Technol.*, 41, 5770–5777, doi:10.1021/es062289b, 2007.
- Allan, J. D., Morgan, W. T., Darbyshire, E., Flynn, M. J., Williams, P. I., Oram, D. E., Artaxo, P., Brito, J., Lee, J. D., and Coe, H.: Airborne observations of IEPOX-derived isoprene SOA in the Amazon during SAMBBA, *Atmos. Chem. Phys.*, 14, 11393–11407, doi:10.5194/acp-14-11393-2014, 2014.
- Andreae, M. and Rosenfeld, D.: Aerosol–cloud–precipitation interactions, Part I. The nature and sources of cloud-active aerosols, *Earth-Sci. Rev.*, 89, 13–41, doi:10.1016/j.earscirev.2008.03.001, 2008.
- Andreae, M. O., Artaxo, P., Brandão, C., Carswell, F. E., Ciccioli, P., Da Costa, A. L., Gulf, A. D., Esteves, J. L., Gash, J. H. C., Grace, J., Kabat, P., Lelieveld, J., Malhi, Y., Manzi, A. O., Meixner, F. X., Nobre, A. D., Nobre, C., Ruivo, M. D. L. P., Silva-Dias, M. A., Stefani, P., Valentini, R., Von Jouanne, J., and Waterloo, M. J.: Biogeochemical cycling of carbon, water, energy, trace gases, and aerosols in Amazonia: The LBA-EUSTACH experiments, *J. Geophys. Res.-Atmos.*, 107, 8066, doi:10.1029/2001JD000524, 2002.
- Andreae, M. O., Rosenfeld, D., Artaxo, P., Costa, A. A., Frank, G. P., Longo, K. M., and Silva-Dias, M. A. F.: Smoking rain clouds over the Amazon, *Science*, 303, 1337–1342, doi:10.1126/science.1092779, 2004.
- Andreae, M. O., Acevedo, O. C., Araújo, A., Artaxo, P., Barbosa, C. G. G., Barbosa, H. M. J., Brito, J., Carbone, S., Chi, X., Cintra, B. B. L., da Silva, N. F., Dias, N. L., Dias-Júnior, C. Q., Ditas, F., Ditz, R., Godoi, A. F. L., Godoi, R. H. M., Heimann, M., Hoffmann, T., Kesselmeier, J., Könemann, T., Krüger, M. L., Lavric, J. V., Manzi, A. O., Lopes, A. P., Martins, D. L., Mikhailov, E. F., Moran-Zuloaga, D., Nelson, B. W., Nölscher, A. C., Santos Nogueira, D., Piedade, M. T. F., Pöhlker, C., Pöschl, U., Quesada, C. A., Rizzo, L. V., Ro, C.-U., Ruckteschler, N., Sá, L. D. A., de Oliveira Sá, M., Sales, C. B., dos Santos, R. M. N., Saturno, J., Schöngart, J., Sörgel, M., de Souza, C. M., de Souza, R. A. F., Su, H., Targhetta, N., Tóta, J., Trebs, I., Trumbore, S., van Eijck, A., Walter, D., Wang, Z., Weber, B., Williams, J., Winderlich, J., Wittmann, F., Wolff, S., and Yáñez-Serrano, A. M.: The Amazon Tall Tower Observatory (ATTO): overview of pilot measurements on ecosystem ecology, meteorology, trace gases, and aerosols, *Atmos. Chem. Phys.*, 15, 10723–10776, doi:10.5194/acp-15-10723-2015, 2015.
- Artaxo, P., Rizzo, L. V., Brito, J. F., Barbosa, H. M. J., Arana, A., Sena, E. T., Cirino, G. G., Bastos, W., Martin, S. T., and Andreae, M. O.: Atmospheric aerosols in Amazonia and land use change: from natural biogenic to biomass burning conditions, *Faraday Discuss.*, 165, 203–235, doi:10.1039/c3fd00052d, 2013.
- Ben-Ami, Y., Koren, I., Rudich, Y., Artaxo, P., Martin, S. T., and Andreae, M. O.: Transport of North African dust from the Bodélé depression to the Amazon Basin: a case study, *Atmos. Chem. Phys.*, 10, 7533–7544, doi:10.5194/acp-10-7533-2010, 2010.
- Brito, J., Rizzo, L. V., Morgan, W. T., Coe, H., Johnson, B., Haywood, J., Longo, K., Freitas, S., Andreae, M. O., and Artaxo, P.: Ground-based aerosol characterization during the South American Biomass Burning Analysis (SAMBBA) field experiment, *Atmos. Chem. Phys.*, 14, 12069–12083, doi:10.5194/acp-14-12069-2014, 2014.
- Chen, Q., Farmer, D. K., Schneider, J., Zorn, S. R., Heald, C. L., Karl, T. G., Guenther, A., Allan, J. D., Robinson, N., Coe, H., Kimmel, J. R., Pauliquevis, T., Borrmann, S., Pöschl, U., Andreae, M. O., Artaxo, P., Jimenez, J. L., and Martin, S. T.: Mass spectral characterization of submicron biogenic organic particles in the Amazon Basin, *Geophys. Res. Lett.*, 36, L20806, doi:10.1029/2009GL039880, 2009.
- Chen, Q., Farmer, D. K., Rizzo, L. V., Pauliquevis, T., Kuwata, M., Karl, T. G., Guenther, A., Allan, J. D., Coe, H., Andreae, M. O., Pöschl, U., Jimenez, J. L., Artaxo, P., and Martin, S. T.: Submicron particle mass concentrations and sources in the Amazonian wet season (AMAZE-08), *Atmos. Chem. Phys.*, 15, 3687–3701, doi:10.5194/acp-15-3687-2015, 2015.
- Crawford, I., Robinson, N. H., Flynn, M. J., Foot, V. E., Gallagher, M. W., Huffman, J. A., Stanley, W. R., and Kaye, P. H.: Characterisation of bioaerosol emissions from a Colorado pine forest: results from the BEACHON-RoMBAS experiment, *Atmos. Chem. Phys.*, 14, 8559–8578, doi:10.5194/acp-14-8559-2014, 2014.
- Crawford, I., Ruske, S., Topping, D. O., and Gallagher, M. W.: Evaluation of hierarchical agglomerative cluster analysis methods for discrimination of primary biological aerosol, *Atmos. Meas. Tech.*, 8, 4979–4991, doi:10.5194/amt-8-4979-2015, 2015.

- Crawford, I., Lloyd, G., Herrmann, E., Hoyle, C. R., Bower, K. N., Connolly, P. J., Flynn, M. J., Kaye, P. H., Choulaton, T. W., and Gallagher, M. W.: Observations of fluorescent aerosol–cloud interactions in the free troposphere at the High-Altitude Research Station Jungfraujoch, *Atmos. Chem. Phys.*, 16, 2273–2284, doi:10.5194/acp-16-2273-2016, 2016.
- Cubison, M., Coe, H., and Gysel, M.: A modified hygroscopic tandem DMA and a data retrieval method based on optimal estimation, *J. Aerosol Sci.*, 36, 846–865, doi:10.1016/j.jaerosci.2004.11.009, 2005.
- Cubison, M. J., Ortega, A. M., Hayes, P. L., Farmer, D. K., Day, D., Lechner, M. J., Brune, W. H., Apel, E., Diskin, G. S., Fisher, J. A., Fuelberg, H. E., Hecobian, A., Knapp, D. J., Mikoviny, T., Riemer, D., Sachse, G. W., Sessions, W., Weber, R. J., Weinheimer, A. J., Wisthaler, A., and Jimenez, J. L.: Effects of aging on organic aerosol from open biomass burning smoke in aircraft and laboratory studies, *Atmos. Chem. Phys.*, 11, 12049–12064, doi:10.5194/acp-11-12049-2011, 2011.
- Draxler, R. and Hess, G.: An Overview of the HYSPLIT_4 Modelling System for Trajectories, Dispersion, and Deposition, *Aust. Meteorol. Mag.*, 47, 295–308, 1998.
- Duplissy, J., Gysel, M., Sjogren, S., Meyer, N., Good, N., Kammermann, L., Michaud, V., Weigel, R., Martins dos Santos, S., Gruening, C., Villani, P., Laj, P., Sellegri, K., Metzger, A., McFiggans, G. B., Wehrle, G., Richter, R., Dommen, J., Ristovski, Z., Baltensperger, U., and Weingartner, E.: Intercomparison study of six HTDMAs: results and recommendations, *Atmos. Meas. Tech.*, 2, 363–378, doi:10.5194/amt-2-363-2009, 2009.
- Elbert, W., Taylor, P. E., Andreae, M. O., and Pöschl, U.: Contribution of fungi to primary biogenic aerosols in the atmosphere: wet and dry discharged spores, carbohydrates, and inorganic ions, *Atmos. Chem. Phys.*, 7, 4569–4588, doi:10.5194/acp-7-4569-2007, 2007.
- Fleming, Z. L., Monks, P. S., and Manning, A. J.: Review: Untangling the influence of air-mass history in interpreting observed atmospheric composition, *Atmos. Res.*, 104–105, 1–39, doi:10.1016/j.atmosres.2011.09.009, 2012.
- Foot, V. E., Kaye, P. H., Stanley, W. R., Barrington, S. J., Gallagher, M., and Gabey, A.: Low-cost real-time multiparameter bio-aerosol sensors, in: Proceedings of SPIE, edited by: Carrano, J. C. and Zukauskas, A., 7116, 71160I–71160I-12, doi:10.1117/12.800226, 2008.
- Formenti, P., Andreae, M. O., Lange, L., Roberts, G., Cafmeyer, J., Rajta, I., Maenhaut, W., Holben, B. N., Artaxo, P., and Lelieveld, J.: Saharan dust in Brazil and Suriname during the Large-Scale Biosphere-Atmosphere Experiment in Amazonia (LBA) – Cooperative LBA Regional Experiment (CLAIRE) in March 1998, *J. Geophys. Res.*, 106, 14919, doi:10.1029/2000JD900827, 2001.
- Gabey, A. M., Gallagher, M. W., Whitehead, J., Dorsey, J. R., Kaye, P. H., and Stanley, W. R.: Measurements and comparison of primary biological aerosol above and below a tropical forest canopy using a dual channel fluorescence spectrometer, *Atmos. Chem. Phys.*, 10, 4453–4466, doi:10.5194/acp-10-4453-2010, 2010.
- Gabey, A. M., Stanley, W. R., Gallagher, M. W., and Kaye, P. H.: The fluorescence properties of aerosol larger than 0.8 μm in urban and tropical rainforest locations, *Atmos. Chem. Phys.*, 11, 5491–5504, doi:10.5194/acp-11-5491-2011, 2011.
- Gilbert, G. S. and Reynolds, D. R.: Nocturnal fungi: Airborne spores in the canopy and understory of a tropical rain forest, *Biotropica*, 37, 462–464, doi:10.1111/j.1744-7429.2005.00061.x, 2005.
- Good, N., Coe, H., and McFiggans, G.: Instrumentational operation and analytical methodology for the reconciliation of aerosol water uptake under sub- and supersaturated conditions, *Atmos. Meas. Tech.*, 3, 1241–1254, doi:10.5194/amt-3-1241-2010, 2010.
- Graham, B.: Composition and diurnal variability of the natural Amazonian aerosol, *J. Geophys. Res.*, 108, 4765, doi:10.1029/2003JD004049, 2003.
- Gunthe, S. S., King, S. M., Rose, D., Chen, Q., Roldin, P., Farmer, D. K., Jimenez, J. L., Artaxo, P., Andreae, M. O., Martin, S. T., and Pöschl, U.: Cloud condensation nuclei in pristine tropical rainforest air of Amazonia: size-resolved measurements and modeling of atmospheric aerosol composition and CCN activity, *Atmos. Chem. Phys.*, 9, 7551–7575, doi:10.5194/acp-9-7551-2009, 2009.
- Gysel, M., McFiggans, G., and Coe, H.: Inversion of tandem differential mobility analyser (TDMA) measurements, *J. Aerosol Sci.*, 40, 134–151, doi:10.1016/j.jaerosci.2008.07.013, 2009.
- Healy, D. A., Huffman, J. A., O'Connor, D. J., Pöhlker, C., Pöschl, U., and Sodeau, J. R.: Ambient measurements of biological aerosol particles near Killarney, Ireland: a comparison between real-time fluorescence and microscopy techniques, *Atmos. Chem. Phys.*, 14, 8055–8069, doi:10.5194/acp-14-8055-2014, 2014.
- Hernandez, M., Perring, A., McCabe, K., Kok, G., Granger, G., and Baumgardner, D.: Composite Catalogues of Optical and Fluorescent Signatures Distinguish Bioaerosol Classes, *Atmos. Meas. Tech. Discuss.*, doi:10.5194/amt-2015-372, in review, 2016.
- Huffman, J. A., Sinha, B., Garland, R. M., Snee-Pollmann, A., Gunthe, S. S., Artaxo, P., Martin, S. T., Andreae, M. O., and Pöschl, U.: Size distributions and temporal variations of biological aerosol particles in the Amazon rainforest characterized by microscopy and real-time UV-APS fluorescence techniques during AMAZE-08, *Atmos. Chem. Phys.*, 12, 11997–12019, doi:10.5194/acp-12-11997-2012, 2012.
- Irwin, M., Robinson, N., Allan, J. D., Coe, H., and McFiggans, G.: Size-resolved aerosol water uptake and cloud condensation nuclei measurements as measured above a Southeast Asian rainforest during OP3, *Atmos. Chem. Phys.*, 11, 11157–11174, doi:10.5194/acp-11-11157-2011, 2011.
- Jones, A. M. and Harrison, R. M.: The effects of meteorological factors on atmospheric bioaerosol concentrations – a review, *Sci. Total Environ.*, 326, 151–180, doi:10.1016/j.scitotenv.2003.11.021, 2004.
- Kaye, P. H., Stanley, W. R., Hirst, E., Foot, E. V., Baxter, K. L., and Barrington, S. J.: Single particle multichannel bio-aerosol fluorescence sensor, *Opt. Express*, 13, 3583–3593, 2005.
- Krejci, R., Ström, J., de Reus, M., Williams, J., Fischer, H., Andreae, M. O., and Hansson, H.-C.: Spatial and temporal distribution of atmospheric aerosols in the lowermost troposphere over the Amazonian tropical rainforest, *Atmos. Chem. Phys.*, 5, 1527–1543, doi:10.5194/acp-5-1527-2005, 2005.
- Martin, S. T., Andreae, M. O., Althausen, D., Artaxo, P., Baars, H., Borrmann, S., Chen, Q., Farmer, D. K., Guenther, A., Gunthe, S. S., Jimenez, J. L., Karl, T., Longo, K., Manzi, A., Müller, T., Pauliquevis, T., Petters, M. D., Prenni, A. J., Pöschl, U., Rizzo, L. V., Schneider, J., Smith, J. N., Swietlicki, E., Tota, J., Wang,

- J., Wiedensohler, A., and Zorn, S. R.: An overview of the Amazonian Aerosol Characterization Experiment 2008 (AMAZE-08), *Atmos. Chem. Phys.*, 10, 11415–11438, doi:10.5194/acp-10-11415-2010, 2010a.
- Martin, S. T., Andreae, M. O., Artaxo, P., Baumgardner, D., Chen, Q., Goldstein, A. H., Guenther, A., Heald, C. L., Mayol-Bracero, O. L., McMurry, P. H., Pauliquevis, T., Pöschl, U., Prather, K. A., Roberts, G. C., Saleska, S. R., Silva Dias, M. A., Spracklen, D. V., Swietlicki, E., and Trebs, I.: Sources and properties of Amazonian aerosol particles, *Rev. Geophys.*, 48, RG2002, doi:10.1029/2008RG000280, 2010b.
- Massling, A., Niedermeier, N., Hennig, T., Fors, E. O., Swietlicki, E., Ehn, M., Hämeri, K., Villani, P., Laj, P., Good, N., McFiggans, G., and Wiedensohler, A.: Results and recommendations from an intercomparison of six Hygroscopicity-TDMA systems, *Atmos. Meas. Tech.*, 4, 485–497, doi:10.5194/amt-4-485-2011, 2011
- Perring, A. E., Schwarz, J. P., Baumgardner, D., Hernandez, M. T., Spracklen, D. V., Heald, C. L., Gao, R. S., Kok, G., McMeeking, G. R., McQuaid, J. B., and Fahey, D. W.: Airborne observations of regional variation in fluorescent aerosol across the United States, *J. Geophys. Res.-Atmos.*, 120, 1153–1170, doi:10.1002/2014JD022495, 2015.
- Petters, M. D. and Kreidenweis, S. M.: A single parameter representation of hygroscopic growth and cloud condensation nucleus activity, *Atmos. Chem. Phys.*, 7, 1961–1971, doi:10.5194/acp-7-1961-2007, 2007.
- Pöhlker, C., Huffman, J. A., and Pöschl, U.: Autofluorescence of atmospheric bioaerosols – fluorescent biomolecules and potential interferences, *Atmos. Meas. Tech.*, 5, 37–71, doi:10.5194/amt-5-37-2012, 2012.
- Pöschl, U., Martin, S. T., Sinha, B., Chen, Q., Gunthe, S. S., Huffman, J. A., Borrmann, S., Farmer, D. K., Garland, R. M., Helas, G., Jimenez, J. L., King, S. M., Manzi, A., Mikhailov, E., Pauliquevis, T., Petters, M. D., Prenni, A. J., Roldin, P., Rose, D., Schneider, J., Su, H., Zorn, S. R., Artaxo, P., and Andreae, M. O.: Rainforest aerosols as biogenic nuclei of clouds and precipitation in the Amazon, *Science*, 329, 1513–1516, doi:10.1126/science.1191056, 2010.
- Prenni, A. J., Petters, M. D., Kreidenweis, S. M., Heald, C. L., Martin, S. T., Artaxo, P., Garland, R. M., Wollny, A. G., and Pöschl, U.: Relative roles of biogenic emissions and Saharan dust as ice nuclei in the Amazon basin, *Nat. Geosci.*, 2, 402–405, 2009.
- Reutter, P., Su, H., Trentmann, J., Simmel, M., Rose, D., Gunthe, S. S., Wernli, H., Andreae, M. O., and Pöschl, U.: Aerosol- and updraft-limited regimes of cloud droplet formation: influence of particle number, size and hygroscopicity on the activation of cloud condensation nuclei (CCN), *Atmos. Chem. Phys.*, 9, 7067–7080, doi:10.5194/acp-9-7067-2009, 2009.
- Rissler, J., Swietlicki, E., Zhou, J., Roberts, G., Andreae, M. O., Gatti, L. V., and Artaxo, P.: Physical properties of the submicrometer aerosol over the Amazon rain forest during the wet-to-dry season transition – comparison of modeled and measured CCN concentrations, *Atmos. Chem. Phys.*, 4, 2119–2143, doi:10.5194/acp-4-2119-2004, 2004
- Rissler, J., Vestin, A., Swietlicki, E., Fisch, G., Zhou, J., Artaxo, P., and Andreae, M. O.: Size distribution and hygroscopic properties of aerosol particles from dry-season biomass burning in Amazonia, *Atmos. Chem. Phys.*, 6, 471–491, doi:10.5194/acp-6-471-2006, 2006.
- Rizzo, L. V., Artaxo, P., Müller, T., Wiedensohler, A., Paixão, M., Cirino, G. G., Arana, A., Swietlicki, E., Roldin, P., Fors, E. O., Wiedemann, K. T., Leal, L. S. M., and Kulmala, M.: Long term measurements of aerosol optical properties at a primary forest site in Amazonia, *Atmos. Chem. Phys.*, 13, 2391–2413, doi:10.5194/acp-13-2391-2013, 2013.
- Roberts, G. C. and Nenes, A.: A Continuous-Flow Streamwise Thermal-Gradient CCN Chamber for Atmospheric Measurements, *Aerosol Sci. Technol.*, 39, 206–221, doi:10.1080/027868290913988, 2005.
- Robinson, N. H., Newton, H. M., Allan, J. D., Irwin, M., Hamilton, J. F., Flynn, M., Bower, K. N., Williams, P. I., Mills, G., Reeves, C. E., McFiggans, G., and Coe, H.: Source attribution of Bornean air masses by back trajectory analysis during the OP3 project, *Atmos. Chem. Phys.*, 11, 9605–9630, doi:10.5194/acp-11-9605-2011, 2011.
- Robinson, N. H., Allan, J. D., Huffman, J. A., Kaye, P. H., Foot, V. E., and Gallagher, M.: Cluster analysis of WIBS single-particle bioaerosol data, *Atmos. Meas. Tech.*, 6, 337–347, doi:10.5194/amt-6-337-2013, 2013.
- Schneider, J., Freutel, F., Zorn, S. R., Chen, Q., Farmer, D. K., Jimenez, J. L., Martin, S. T., Artaxo, P., Wiedensohler, A., and Borrmann, S.: Mass-spectrometric identification of primary biological particle markers and application to pristine submicron aerosol measurements in Amazonia, *Atmos. Chem. Phys.*, 11, 11415–11429, doi:10.5194/acp-11-11415-2011, 2011
- Schroeder, W., Prins, E., Giglio, L., Csiszar, I., Schmidt, C., Morisette, J., and Morton, D.: Validation of GOES and MODIS active fire detection products using ASTER and ETM+ data, *Remote Sens. Environ.*, 112, 2711–2726, doi:10.1016/j.rse.2008.01.005, 2008.
- Spracklen, D. V. and Heald, C. L.: The contribution of fungal spores and bacteria to regional and global aerosol number and ice nucleation immersion freezing rates, *Atmos. Chem. Phys.*, 14, 9051–9059, doi:10.5194/acp-14-9051-2014, 2014.
- Stanley, W. R., Kaye, P. H., Foot, V. E., Barrington, S. J., Gallagher, M., and Gabey, A.: Continuous bioaerosol monitoring in a tropical environment using a UV fluorescence particle spectrometer, *Atmos. Sci. Lett.*, 12, 195–199, doi:10.1002/asl.310, 2011.
- Swietlicki, E., Hansson, H.-C., Hämeri, K., Svenningsson, B., Massling, A., McFiggans, G. B., McMurry, P. H., Petäjä, T., Tunved, P., Gysel, M., Topping, D., Weingartner, E., Baltensperger, U., Rissler, J., Wiedensohler, A., and Kulmala, M.: Hygroscopic properties of submicrometer atmospheric aerosol particles measured with H-TDMA instruments in various environments – a review, *Tellus B*, 60, 432–469, 2008.
- Topping, D. O., McFiggans, G. B., and Coe, H.: A curved multi-component aerosol hygroscopicity model framework: Part 1 – Inorganic compounds, *Atmos. Chem. Phys.*, 5, 1205–1222, doi:10.5194/acp-5-1205-2005, 2005.
- Toprak, E. and Schnaiter, M.: Fluorescent biological aerosol particles measured with the Waveband Integrated Bioaerosol Sensor WIBS-4: laboratory tests combined with a one year field study, *Atmos. Chem. Phys.*, 13, 225–243, doi:10.5194/acp-13-225-2013, 2013.
- Tuch, T. M., Haudek, A., Müller, T., Nowak, A., Wex, H., and Wiedensohler, A.: Design and performance of an automatic

- regenerating adsorption aerosol dryer for continuous operation at monitoring sites, *Atmos. Meas. Tech.*, 2, 417–422, doi:10.5194/amt-2-417-2009, 2009.
- Vestin, A., Rissler, J., Swietlicki, E., Frank, G. P., and Andreae, M. O.: Cloud-nucleating properties of the Amazonian biomass burning aerosol: Cloud condensation nuclei measurements and modeling, *J. Geophys. Res.*, 112, D14201, doi:10.1029/2006JD008104, 2007.
- Whitehead, J. D., Gallagher, M. W., Dorsey, J. R., Robinson, N., Gabey, A. M., Coe, H., McFiggans, G., Flynn, M. J., Ryder, J., Nemitz, E., and Davies, F.: Aerosol fluxes and dynamics within and above a tropical rainforest in South-East Asia, *Atmos. Chem. Phys.*, 10, 9369–9382, doi:10.5194/acp-10-9369-2010, 2010.
- Whitehead, J. D., Irwin, M., Allan, J. D., Good, N., and McFiggans, G.: A meta-analysis of particle water uptake reconciliation studies, *Atmos. Chem. Phys.*, 14, 11833–11841, doi:10.5194/acp-14-11833-2014, 2014.
- Worobiec, A., Szalóki, I., Osán, J., Maenhaut, W., Stefaniak, E. A., and Van Grieken, R.: Characterisation of Amazon Basin aerosols at the individual particle level by X-ray microanalytical techniques, *Atmos. Environ.*, 41, 9217–9230, doi:10.1016/j.atmosenv.2007.07.056, 2007.
- Zhang, Z., Engling, G., Zhang, L., Kawamura, K., Yang, Y., Tao, J., Zhang, R., Chan, C.-Y., and Li, Y.: Significant influence of fungi on coarse carbonaceous and potassium aerosols in a tropical rainforest, *Environ. Res. Lett.*, 10, 034015, doi:10.1088/1748-9326/10/3/034015, 2015.
- Zhou, J., Swietlicki, E., Hansson, H. C., and Artaxo, P.: Submicrometer aerosol particle size distribution and hygroscopic growth measured in the Amazon rain forest during the wet season, *J. Geophys. Res.*, 107, 8055, doi:10.1029/2000JD000203, 2002.